Time-Division Multiplexing for Power and Data Transmission on Optical Fibers

Oscar López-Lapeña, *Member, IEEE*, and Jose Polo-Cantero

***Abstract*—Internet of Things (IoT) raises the interconnection of low-cost sensor nodes networks everywhere even in harsh environments where conventional power supply systems and communication channels are not feasible. Power over Fiber is an alternative solution but its implementation costs are sometimes too high because of the optical devices involved. This article proposes a time-division multiplexing control algorithm and a circuit design to share the same laser diode and photodiode for power and downstream data transmission. This is a feasible solution to reduce implementation costs when sensor nodes require downstream data rates much lower than the capacity of the link.**

***Index Terms*—Internet of Things (IoT), low-power electronics, Power over Fiber (PoF), sensor network, time-division multiplexing.**

I. Introduction

NOWADAYS more and more devices are connected to the Internet conforming Internet of Things (IoT). The most important core of devices that have joined the Internet rush is sensors. They are in every area of our lives, from environmental measurements, to monitoring transport services, smart agriculture [1], patients health, electric, gas or water utilities [2], or detection of underwater objects for navigation applications [3]. These sensors are integrated into remote nodes that need to be powered and need to transmit data abroad somehow.

Conventionally data transmission is carried out using electric conductor or radio-frequency waves. However, there are situations where it is not possible or even dangerous for the use of these communication channels. In applications, such as high voltages transmission lines supervision, bioelectric measurements, and gas pipeline monitoring, electrical conductors or radio signals can form a path for electromagnetic interferences (EMI), electric shocks, or cause explosion ignitions, respectively. In other mediums, such as submarine or buried facilities, the high radio wave absorption makes this communication medium usually unfeasible.

Power supply is another design challenge when the power grid is not available next to sensor nodes and the use of primary batteries leads to unacceptable operating times. In these cases, energy harvesting offers sometimes a way to supply nodes, but there are situations where there is no a proper energy source available in the environment and it must be remotely supplied using power transmission lines.

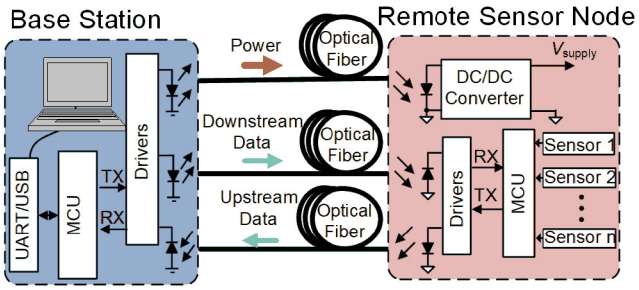

Fig. 1. Architecture of a conventional PoF remote sensor node.

A feasible solution consists of substituting antennas or copper cables with optical fibers. Power-over-Fiber (PoF) sensors use optical fibers for both communication and power transmission. In contrast to copper cables, optical fibers are lighter, thinner, less vulnerable to corrosion, invulnerable to EMI, and form galvanic isolation channels. Several works have been published that uses PoF in applications, such as power grid stations monitoring [2], [4], [5], gas concentration sensing [6], [7], submarine sensors [8], [9], industrial harsh environments [10]–[12], or bioelectric measurements [13]. Nevertheless, this technology still presents several design challenges due to its high cost, power transmission restrictions, and interaction with data transmission. The costs are mainly given by optical components, such as high power lasers (HPLs), photodiodes (PDs), and optical fibers. Conventional PoFs use separate optical components to transmit power and data (see Fig. 1), hence, the cost is higher than a conventional communication optical link. Other proposals intended to reduce the cost of fibers using wavelength-division multiplexing [14] or spatial division multiplexing with multicore fibers [15], but they do not reduce the number of HPLs and PDs that are required.

Budelmann [10] proposed to reduce costs substituting HPLs with cheaper light-emitting diodes (LEDs). Their lower power efficiency and poor optical coupling capacity were overcome using a 1 mm in diameter polymer optical fiber and low-power sensor nodes. In addition to reducing the costs, the resulting irradiance inside the fibers was below the safety threshold limit to be used in explosive environments. Nevertheless, the high attenuation in such cores limits the transmission length to a few meters and the power supplied to remote sensor node

Manuscript received 5 August 2021; revised 18 February 2022; accepted 14 March 2022. Date of publication 21 March 2022; date of current version 7 September 2022. *(Corresponding author: Oscar López-Lapeña.)*

The authors are with the Department of Electronic Engineering, Universitat Politecnica de Catalunya, 08860 Castelldefels, Spain (e-mail: oscar.lopez@upc.edu; jose.polo@upc.edu).

Digital Object Identifier 10.1109/JIOT.2022.3160977

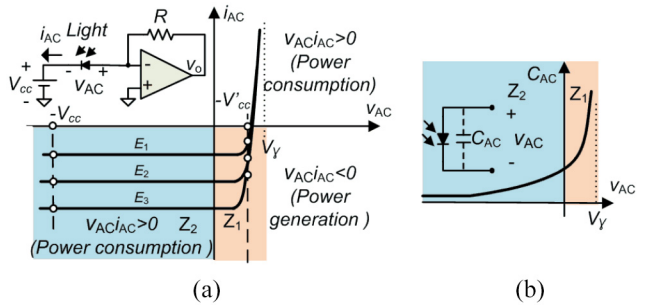

Fig. 2. PD operation regions. (a) Current (i_{AC}) versus voltage (v_{AC}) performance when is connected to a transimpedance amplifier and is submitted to several light irradiations ($E_1 < E_2 < E_3$). (b) Parasite capacitance (C_{AC}) of a PD versus bias voltage (v_{AC}).

to 23 μW. This power level is significantly lower than the power provided by other PoF links described in the literature for IoT applications. Souza *et al.* [12] used a 0.6-W laser to power supply a 152-mW remote node. Nevertheless, such power level is not needed in most of these applications. When low sampling frequencies are required, power consumption can be reduced to hundreds of microwatts using dynamic power management techniques.

This article proposes using a single 2-mW laser diode (LD) and a conventional single silicon PD for power and data transmission. Taking advantage of the fact that low downstream transmission data rates are usually required, a time-division multiplexing scheme is used to alternatively operate in both modes. This operation scheme reduces the number of components and thus, reduces system and installation costs, but implies several technical issues that will be described throughout this article. The need for biasing PDs at different points, depending on their use as communication or powering devices is shown in Section II. This implies the use of a reconfigurable bias circuit that is described in Section III, together with an overall system architecture and operation. The use of this system in several scenarios, such as single node or multinode network, is shown in Section IV. Finally, Section V shows design constraints and experimental results.

II. PD Connection Modes

PDs are p-i-n (*p*, *i*ntrinsic, and *n* doped regions) junction devices that convert light into electrical current. Although they are traditionally used as communication devices, they can also be used to harvest energy as photovoltaic panels. Both modes of operation require different operating regions. The performances versus the bias point are observed in Fig. 2 in which typical I/V and parasite capacitance (C_{AC}) are shown.

When the junction is forward biased and $i_{AC} < 0$ (Z_1 region in Fig. 2), the power consumption is negative ($v_{AC} \cdot i_{AC} < 0$, power supply) and high C_{AC} is achieved. Consequently, it is a proper operating region to harvest energy, but its dynamic is too slow to operate in communication mode. On the other hand, the reverse bias region, $i_{AC} < 0$ and $v_{AC} < 0$, (Z_2 region in Fig. 2) offers small C_{AC} but PDs do not work as a power source ($v_{AC} \cdot i_{AC} > 0$, power load). It is not suitable for energy harvesting, but offers fast dynamics for communication.

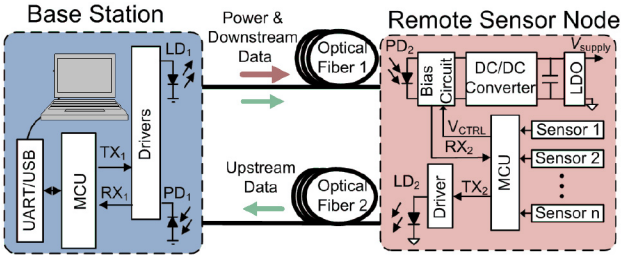

Fig. 3. Proposed architecture for a PoF remote sensor node.

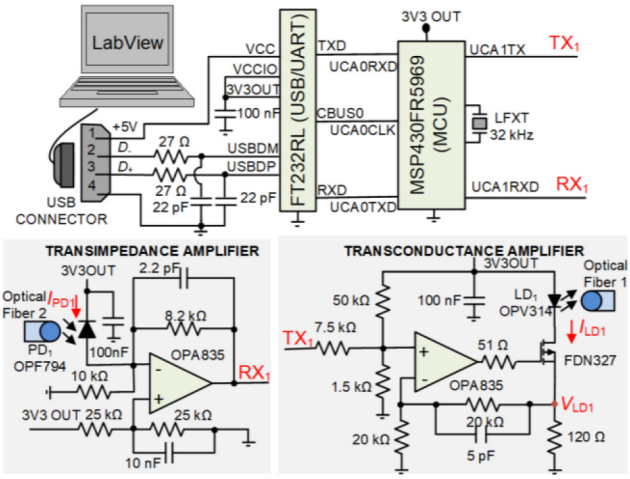

Fig. 4. Scheme of base station.

In the communication mode, the light signal modulates i_{AC} and a transimpedance amplifier (see Fig. 2 in upper left area) transforms it into a voltage signal (v_o) that can be used to bias an input communication port. The use of PDs in Z_2 region results in a wider current range than in Z_1 region and thus, a better signal-to-noise ratio is also achieved.

III. System Architecture

The proposed architecture is depicted in Fig. 3. Unlike the conventional architecture, a single LD in the base station (LD_1) and a single PD in the sensor node (PD_2) are used for power and downstream data transmission through a single optical fiber (Optical Fiber 1). A microcontroller unit (MCU) controls the bias voltage of PD_2 by V_{CTRL} output port to operate in communication or powering modes. Another fiber, LD (LD_2), and PD (PD_1) are used for upstream data transmission. It is also possible to use a single optical fiber for power supply, downstream, and upstream data transmission at the expense of using two optical circulators (see Fig. 10).

In the next sections, a detailed description of each one of the blocks in Fig. 3 is given.

A. Base Station

Base station integrates the user interface, which is implemented by a LabView application in a computer, and an electronic board that is used to communicate and to transmit power through optical fibers (Fig. 4). The electronic board is based on a MCU (MSP430FR5969) that uses a

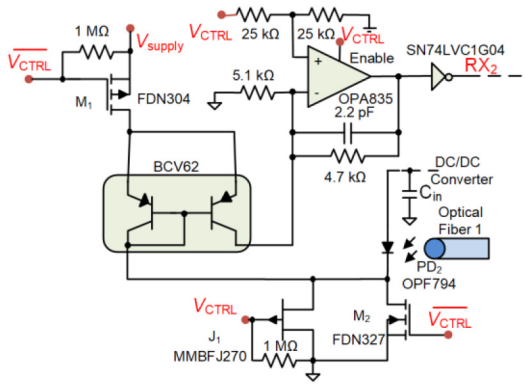

Fig. 5. Configurable PD_2 bias circuit.

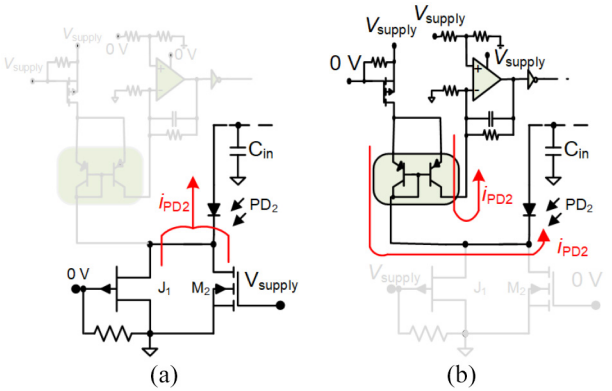

Fig. 6. Bias circuit operation modes. (a) Powering mode (Start-up, $V_{CTRL} = 0$). (b) Communication mode ($V_{CTRL} = V_{supply}$).

USB/Serial converter IC (FT232RL) to communicate with the computer. Furthermore, communication ports in the MCU (UCA1TXD and UCA1RXD, that correspond to TX_1 and RX_1, respectively, in the scheme of Fig. 3) are used to implement the serial communication on the fibers using simple drivers (transimpedance and transconductance amplifiers). The transconductance amplifier drives LD_1 current, I_{LD1}, to $I_{LD1H} = 10.2$ mA when TX1 = 3.3 V and to $I_{LD1L} = 1.3$ mA when TX1 = 0 V. LD_1 was implemented using a 2 mW LD, OPV314. On the other hand, a transimpedance amplifier biases PD_1 at -1.65 V (Z_2 region in Fig. 2) and achieves 24-MHz gain bandwidth.

LDs and PDs drivers have been implemented using general purpose amplifiers (OPA835) for both base station and remote node. Commercial laser drivers or transimpedance amplifier, such as MAX3646 and OPA380, have been dismiss because of its higher power consumption that is caused by its higher bandwidth. As communication rate is delimited by MSP430FR5969, a higher bandwidth is not needed and power consumption reduction has been prioritized.

As different communication schemes are used among computer/base station and base station/remote sensor node, an MCU is needed to implement synchronization algorithms. As we will see in Section III-C, communication with LabView app is started by downstream data frames and uses an accurate clock (12-MHz clock from CBUS0 in FT232RL), while the communication with sensor node is started by upstream data frames and uses an inaccurate clock (digital controlled oscillator (DCO) in the MCU) that needs clock synchronization frames (SYN).

B. Remote Sensor Node

Remote sensor node is formed by a new configurable bias circuit for PD_2 (Fig. 5) and the control, power supply, and laser driver systems (Fig. 7). An MCU (MSP430FR5969) controls the operation mode of bias circuit through V_{CTRL} and $\overline{V_{CTRL}}$ that switch on/off the transistors M_1, M_2, and J_1, and drives serial communication ports (TX_2 = UCA1TXD and RX_2 = UCA1RXD).

Fig. 6 shows the two operation modes of the configurable bias circuit. PD_2 is biased in powering mode when V_{CTRL} is clear ($V_{CTRL} = 0$ V) and $\overline{V_{CTRL}}$ is set ($\overline{V_{CTRL}} = V_{supply}$)

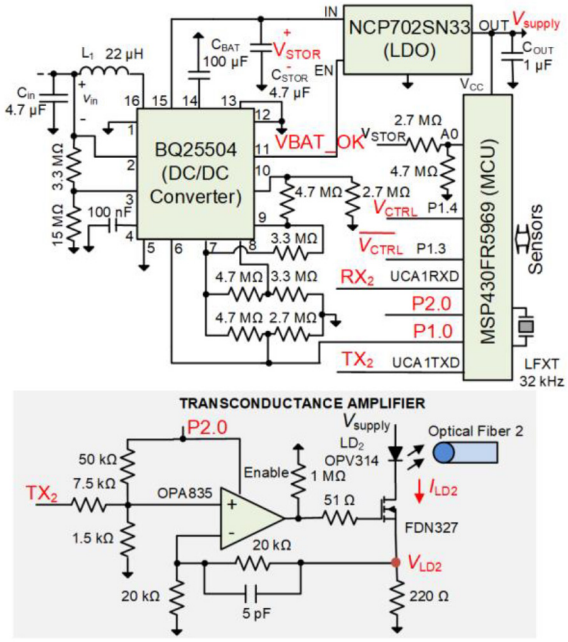

Fig. 7. Control, power supply, and laser driver systems of remote sensor node.

[see Fig. 6(a)]. This operation mode is also achieved during the start-up, when there is no energy to power the MCU and all ports are in high impedance. Initial conduction channel of junction field effect transistor J_1 lets to hold a current conduction path to charge C_{in}. Once MCU is power supplied and $\overline{V_{CTRL}}$ is set, M_2 lets to achieve a higher conduction path increasing power efficiency. In the opposite case, when V_{CTRL} is set and $\overline{V_{CTRL}}$ is clear [see Fig. 6(b)], PD_2 is reverse bias to operate in communication mode. A current mirror (BCV62), a low-power inverter (SN74LVC1G04), and a transimpedance amplifier are used to obtain the proper polarization of RX_2. This scheme lets to achieve 24-MHz gain bandwidth with 650 μA overall current consumption in communication mode, and the consumption is reduced to 2 μA in powering mode.

The power supply system is formed by a low-power boost switching converter (BQ25504) and a low-dropout voltage regulator (LDO) (NCP720SN33) (see Fig. 7). BQ22504 operates from input voltages so low as 330 mV and charges C_{STOR}

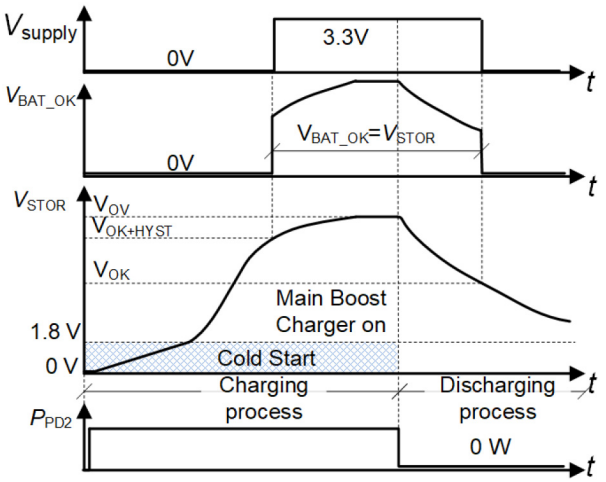

Fig. 8. Power supply operation during start up and after incoming power from PD_2 (P_{PD2}) falls to zero.

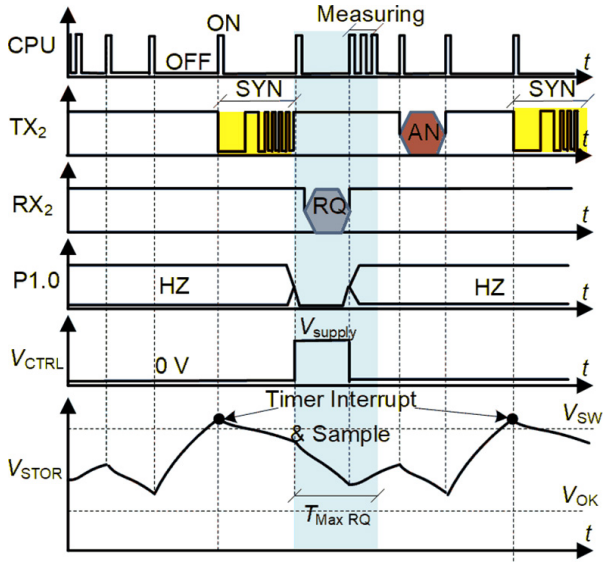

Fig. 9. Powering and transmission data modes scheduling in sensor node.

and C_{BAT}, from stored energy in C_{in}. In order to obtain the maximum power from PD_2, it is polarized at the maximum power point bias voltage (V_{MPP}). This voltage is obtained from the open circuit voltage (V_{OC}) of the PD_2. Every 2 s, PD_2 is momentarily left in open circuit to capture V_{OC} and calculate V_{MPP} as $0.8 \cdot V_{OC}$ (empirical relation in photovoltaic devices). The switching converter transmits the energy from C_{in} to C_{STOR} to hold input capacitor voltage (V_{in}) that it is the PD_2's bias voltage in powering mode, around this optimum value.

Fig. 8 shows the time evolution of the output voltage of LDO (V_{supply}), V_{STOR}, and the control signal V_{BAT_OK} (see Fig. 7). During the start-up, when PD_2 is illuminated and provides a positive power (zone Z_1 in Fig. 2), V_{STOR} rises up reaching several threshold values, V_{OK}, $V_{OK+HYST}$, and V_{OV}, that are set by resistors connected to BQ25504. Until V_{STOR} reaches 1.8 V, BQ25504 operates in cold start mode increasing V_{STOR} very slowly, because of the converter's low power efficiency. Over this limit, the efficiency increases speeding up the charging process. Once $V_{OK+HYST}$ is surpassed, V_{BAT_OK} is set and LDO is turned on to regulate V_{supply} to 3.3 V. The charging process finishes when V_{STOR} reaches the over voltage limit V_{OV}. On the other hand, V_{STOR} falls down when PD_2 is not illuminated ($P_{PD2} = 0$) and LDO is turned off when V_{STOR} falls below V_{OK}.

A transconductance amplifier (see Fig. 7), similar to the one used in the base station, is used to bias LD_2 to transmit data from the remote sensor node. Different resistors are used for both amplifiers because different current ranges are required ($I_{LD2H} = 5.6$ mA and $I_{LD2L} = 0.7$ mA). A high bias current is needed in LD_1 to achieve maximum power transmission. Nevertheless, the bias current of LD_2 must be as low as possible to save power consumption in the sensor node. P2.0 MCU output port lets also to disable OPA835 when no data are transmitted reducing current consumption below 1 μA.

C. Powering and Communication Scheduling

The base station and the remote sensor node must be synchronized to hold powering and communication modes on the same optical devices. This lets to reduce the number of components and, together with the premise of low power consumption of sensor node, to reduce implementation costs.

In order to achieve minimum energy consumption, a high-baud communication rate is needed and sensor node's devices must be hold in sleep-mode for as long as possible. A high communication rate leads to minimum energy consumption during each transmission through LD_2 and maximum duty cycle of PD_2 in powering mode.

The central processing unit (CPU) of the MCU of the sensor node is just active when required and goes back to sleep mode once the work has been completed. A 32-kHz low-power clock (LFXT) is always active and drives a timer that invokes an interrupt service periodically to sample and compare V_{STOR} with a threshold value without waking up the CPU. If this voltage level is over a threshold value V_{SW} (see Fig. 9) that is software set between $V_{OK+HYST}$ and V_{OK}, it means that C_{STOR} has enough energy to perform a measurement. In this case, the CPU is waken up and transmits a synchronization frame (SYN) to the base station through TX_2 (see Fig. 9). This frame follows a sequence pattern (ten "0" + 55 h) and uses the automatic baud-rate detection of UART module in MSP430FR5969. This lets to automatically set the baud rate of UART module of the MCU in the base station. Both UART modules are driven by the DCO in the MCUs whose frequency has a large temperature drift and tolerance. Therefore, automatic baud rate is needed to match the frequency of both serial asynchronous communication modules to avoid errors. The use of high frequency crystal clocks instead of DCO would result in a stable communication frequency; no automatic baud-rate detection would be needed, but would also imply unacceptable energy consumption because of their long stabilization times. However, DCO can be activated or deactivated very fast with low energy cost transition. That lets MCU set DCO at 16 MHz holding a baud-rate around 1 Mb/s during communication periods and turn it off when not needed to save energy.

The reception of the SYN invokes an interrupt service in the base station that wakes up its CPU to transmit the next request (RQ). This transmission is performed inside a maximum time window ($T_{\text{Max RQ}}$), that is delimited by a timer interrupt, in which the PD_2 is biased in communication mode ($V_{\text{CTRL}} = V_{\text{supply}}$). During this time period the switching converter is disabled by setting MCU port P1.0 as an output port at 0 V that changes V_{OV} to 2 V below V_{STOR}. (see Fig. 9).

The reception of RQ by the sensor node or the end limit of the time window invokes an interrupt service that wakes up the CPU to change the bias circuit into powering mode, it enables the switching converter (P1.0 is set in high impedance, HZ, as an input port) and attends the RQ. Once the measurement is performed, the answer (AN) is transmitted back to the base station and C_{STOR} is charged to V_{SW} starting again a new communication cycle.

IV. Communication Scenarios

A master/slave communication model is set between the base station and the sensor node. An RQ is transmitted from the base station formed by a command code and an operand byte, and the AN frames have a payload that can range from 2 to 100 bytes. Frames integrity is checked by the cycle redundant check (CRC) module embedded in MSP430FR5969. The instruction set lets to configure the sensor node and trigger or read the measurements from the sensors attached.

This system is flexible enough to be useful in multiple IoT scenarios just changing the interrupt event that initiates the SYN and incorporating new elements. Following, several examples of system operation are described for various scenarios to demonstrate this flexibility.

A. Single Node With Sensors' Discontinuous Power Supply

The simplest scenario consists of using a single sensor node to perform the measurement of slow signals. The sampling time must be long enough to achieve an energy benefit in disabling sensors' power supply between two consecutive measurements. That lets to turn off the power supply of sensors to save energy and just activate it during the measurements. Once V_{STOR} reaches V_{SW} (interrupt INT), the SYN is transmitted, and the communication and measurement process is performed (see Fig. 10). To simplify the scheme, passive circulators have been used to transmit upstream and downstream frame in a single optical fiber.

Temperature, relative humidity, atmospheric pressure, or other environmental variables are slow signals whose measurements would fit this scenario.

B. Single Node With Sensors' Continuous Power Supply

In some situations, the power supply must be continuously active because the sensor's start-up is longer than the sampling period or there is not an energy consumption benefit in turning it off when it is not used. ECG monitoring is an example in which a very low cut-off frequency input filters implies long start-ups and hence, power supply must be continuously hold on. Fig. 11 shows system operation in this scenario. Power supply is always on and data are periodically sampled and transmitted to a buffer memory using timer interrupts that wakes up the CPU or using a direct memory access (DMA) controller. Once buffer occupancy reaches a threshold value and V_{STOR} is above V_{SW}, node sensor transmits a SYN that initiates communication process to download all data from buffer memory.

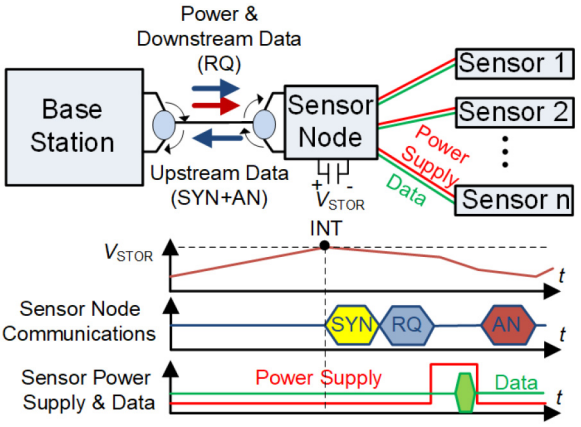

Fig. 10. System operation for a single node with discontinuous power supply.

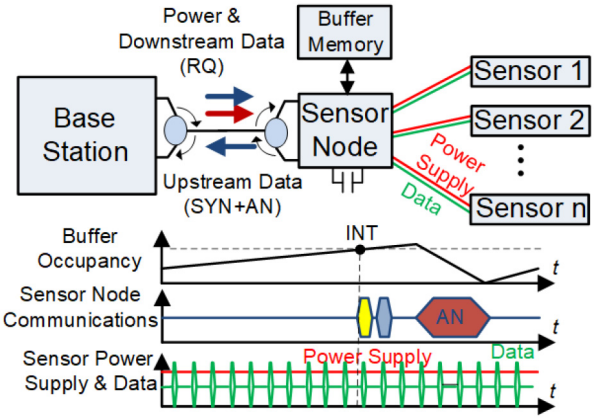

Fig. 11. System operation for a single node with continuous power supply.

C. Multinode Communication

When multiple sensors have to be placed at different locations, several sensor nodes are needed. In order to reduce implementation costs, a single base station and optical fiber can be shared by all of them. A star network topology is defined in which the base station communicates with each sensor node.

Monitoring distribution facilities, such as gas and water pipelines or high voltage distribution lines, are examples of this scenario. Sensors are placed along distribution lines sharing a single optical fiber by using asymmetric optical splitters, as shown in Fig. 12. Splitters must be properly selected to distribute power into nodes according to sensors' power consumption.

In order to avoid collisions, communication frames of sensor nodes are distributed in time slots. The low-power clocks (32 kHz, LFXT) in each sensor node and base station are used to set slots limits. Clocks synchronization is achieved

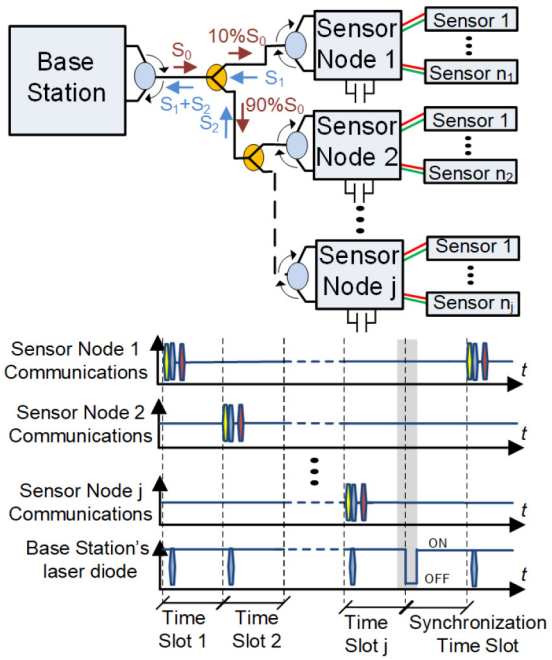

Fig. 12. Multinode communication.

TABLE I
PROTOTYPES PERFORMANCES

Device	Performance	Typical value
General	V_{supply}	3.3 V
	V_{OV}	5.14 V
	$V_{OK+HYST}$	4.95 V
	V_{SW}	4.65 V
	V_{OK}	3.42 V
	I_{LD1H}, I_{LD1L}	10.2 mA, 1.3 mA
	I_{LD2H}, I_{LD2L}	5.6 mA, 0.7 mA
	n_{SYNCH}	14 bits
	n_{AN}	16 bits
	f_{TR}	1 Mbps
BQ25504	η_{SW}	85%
SPC19976 (62.5/125 µm)	γ_{Fiber}	0.3 dB/connector +3 dB/km
OPV314AT (2 mW LD)	η_{LD}	180 µW/mA
	I_{TH}	2 mA
OPF794 (PD)	R_{PD}	0.55 A/W
	V_{OC}	0.65 V

by synchronization signals, which consist on turning LD_1 off periodically during a time interval that is recognized by sensors nodes operating in communication mode. Once a signal is recognized and clocks are synchronized, the following synchronization signals are predictable and sensor nodes enter in communication mode just before starting a new signal. This procedure lets sensor nodes to be in powering mode almost all the time to save energy and to harvest maximum energy.

V. EXPERIMENTAL RESULTS AND DESIGN CONSTRAINTS

To demonstrate that this system works as described, a base station and a sensor node prototype have been implemented using the schemes shown in Figs. 4, 5, and 7. Operating performances are shown in Table I.

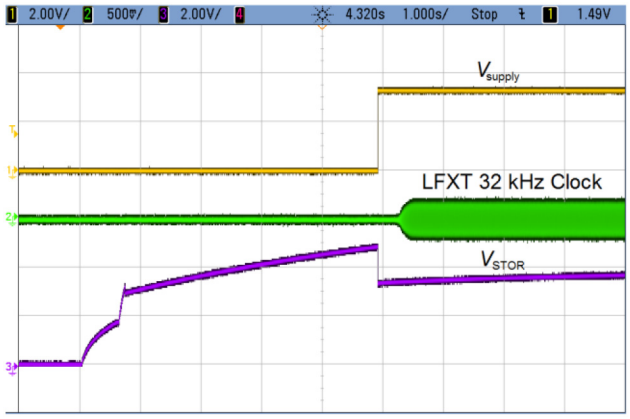

Fig. 13. Experimental system start-up. Horizontal scale is 1 s/division.

These circuits have been connected using the scheme shown in Fig. 3 and a duplex fiber optic cable (SPC19976). An oscilloscope (MSO6054A from Agilent Technologies) has been used to obtain experimental waveforms. In addition to experimentally validating the proposed design, this section shows design constraints, which have also been experimentally verified.

Considering the proposed design, MCU and drivers power consumptions are negligible, and design constraints are deduced for a proper optical devices' selection. LDs, PDs, and optical fiber performances set power available at the input of sensor node as

$$P_{\text{INNode}} = 0.8V_{OC} \cdot \gamma_{\text{Fiber}} \cdot R_{PD} \cdot \eta_{LD}(I_{\text{LD1H}} - I_{TH1}) \quad (1)$$

where R_{PD} is the responsivity of PD_2, and η_{LD} and I_{TH1} are the slope efficiency and the minimum threshold current of LD_1, respectively. Maximum power point bias voltage of PD_2 is calculated as 0.8 V_{OC}, where V_{OC} is its open circuit voltage. I_{LD1H} is the high current level to drive LD_1, and γ_{Fiber} is transmission power efficiency of the optical fiber including connectors losses.

The resulting P_{INNode} is 411 μW and it is higher than the 15 μW that BQ25504 requires to start-up and charge C_{STOR} and C_{BAT}. Once $V_{\text{OK+HYST}}$ is reached, LDO is turned on charging the 1-μF output capacitor (C_{OUT}), supplying the μController and turning on the 32-kHz LFXT clock. Fig. 13 shows that around five seconds are needed to complete the start-up process.

Once start-up finishes, the sensor node is ready to transmit SYN to perform communication. The interrupt event that initiates transmissions depends on the application scenario. Fig. 14 shows V_{STOR}, RX1 and V_{LD1} ($\approx I_{LD1} \cdot 120\ \Omega$) signals for the scenario shown in Section IV-A. A SYN is transmitted each time V_{STOR} reaches V_{SW} and capacitor discharges during measuring and communications processes. In order to prevent V_{STOR} from falling below V_{OK}, the minimum storage capacitances are given by

$$C_{\text{BAT}} + C_{\text{STOR}} > \frac{I_{\text{Sensor}} t_{\text{Sensor}} + \frac{I_{\text{LD2H}}(n_{AN}+n_{\text{SYNCH}})}{f_{TR}}}{V_{SW} - V_{\text{OK}}} \quad (2)$$

where t_{Sensor} is the time that sensors require to start-up and perform the measurement, I_{Sensor} is the average current sensor

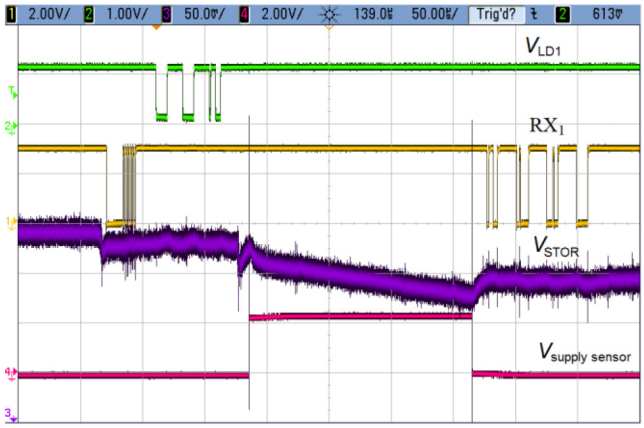

Fig. 14. Communication and power transmission cycle to acquire a slow signal. Sensor's current consumption is 18 mA and it is turned off once the measurement is completed. Horizontal scale 50 μs/division.

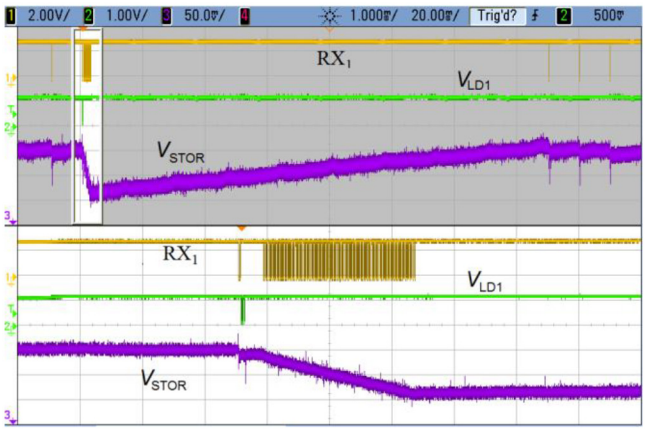

Fig. 15. Communication and power transmission cycles to sample a fast signal. White graph (below) corresponds to a time scale zoom of communication cycle marked with a square in gray graph (above). Horizontal scales are 20 ms/division and 1 ms/division, respectively, for gray and white graphs.

consumption, I_{LD2H} is the high current level to drive LD_2, n_{SYNCH} and n_{AN} are the number of bits of synchronization and response frames, and f_{TR} is communication bitrate. Power transmission during t_{Sensor} and response frame was neglected in this design condition.

This condition limits the measuring charge consumption, $I_{\mathrm{Sensor}}t_{\mathrm{Sensor}}$, to 179 mA·ms for the prototype.

In the scenario described in Section IV-B, sensors are continuously supplied ($t_{\mathrm{Sensor}} = \infty$) and different design constraints must be satisfied. Average sensors' power consumption and transmission data consumption must be lower than the available power at the output of LDO's sensor node. The available power is reduced by power efficiency of switching converter η_{SW} and LDO, and

$$P_{\mathrm{INNode}} \cdot \eta_{SW} \frac{V_{\mathrm{Supply}}}{V_{SW}} > V_{\mathrm{Supply}} \left(\frac{I_{\mathrm{LD2H}}}{f_{TR}} n_{AN} \cdot f_{\mathrm{SAMP}} + I_{\mathrm{Sensor}} \right) \tag{3}$$

where LDO's lowest efficiency was approximated by $V_{\mathrm{Supply}}/V_{SW}$ and f_{SAMP} is the sampling frequency.

Consumption caused by transmission of SYN was neglected because data are saved in a buffer memory and a large number of data bits are transmitted per SYN. For $f_{\mathrm{SAMP}} = 200$ Hz, the maximum consumption of sensor node is 105 μW ($I_{\mathrm{Sensor}} = 32\ \mu$A) for the prototype.

Fig. 15 shows experimental system operation mode in this scenario in which 100 bytes are downloaded from a buffer memory. Assuming a constant sensor current consumption, V_{STOR} falls to its minimum value when data are transmitted. Considering that n_{BUF} is the number of data registers transmitted in each communication frame, the minimum capacitances to avoid V_{STOR} from falling below V_{OK} are given by

$$C_{\mathrm{BAT}} + C_{\mathrm{STOR}} > \frac{\left(I_{\mathrm{Sensor}} - I_{\mathrm{Supply}} + I_{D2H}\right) \frac{n_{AN} \cdot n_{BUF}}{f_{TR}}}{V_{SW} - V_{\mathrm{OK}}} \tag{4}$$

where $I_{\mathrm{Supply}} \approx P_{\mathrm{INNode}} \cdot \eta_{SW}/V_{SW}$.

Finally, a periodic synchronization signal and synchronization routines were programmed in the base station and in the sensor node for multinode communication. Fig. 16 shows experimental communication frames for a five slots multimode scenario. Considering negligible the loss of energy for synchronization signal transmission, the same design constraints must be used but P_{INNode} in (1) is shared by all nodes.

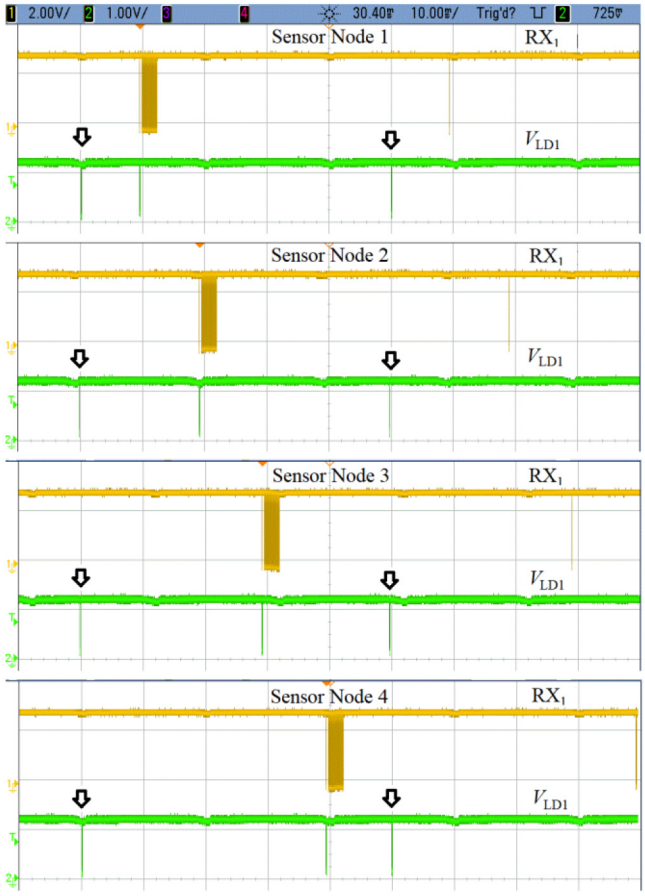

Fig. 16. Communication and powering synchronization for a five slots multinode scenario. Synchronization signals are marked with an arrow. These results have been obtained using a single sensor node configured in each slot, identified as "Sensor Node 1," ..., "Sensor Node 4." Results correspond to four oscilloscope captures synchronized in time by synchronization signals. Horizontal scale 10 ms/division.

VI. Conclusion

The high cost of PoF system can be significantly reduced by using conventional low-power optical devices that are multiplexed for power and data transmission. Whereas PDs must be inverse biased for communication, direct biased is required to harvest energy. A single PD cannot operate in both modes at once and hence, synchronization algorithms and reconfigurable bias circuits are required. A low-cost and low-power solution has been proposed using MSP430FR5969 that lets to communicate and to power supply single nodes and multinode networks. A master/slave communication model has been defined using SYN that delimits sensor nodes' communication states and lets baud-rate synchronization. As automatic baud-rate synchronization is performed in each communication cycle, an accurate clock is not need and a fast start-up internal RC-type DCO is used that can be quickly activate or deactivate, together with the CPU and optical device drivers, to save energy.

A proof-of-concept prototype demonstrated that low-cost 2 mW LDs can be used to continuously power a 105 μW sensor and transmit 16 bits data at 200-Hz sampling frequency. Clearly, higher transmission rates and power consumptions can be achieved using HPLs and PDs. Comparing proposed design with other low-power PoF systems, it is around 50% more expensive than the cheapest design in the literature that was proposed by Budelmann [10], but the available power to supply sensor nodes is almost eighteen times higher. Moreover, thinner optical fibers can be used with a lower attenuation factor.

Time slot switching, which is conventionally used as a medium-access communication protocol in optical fiber networks, can also be used to coordinate powering and communication states in multinode PoF systems.

References

[1] O. Friha, M. A. Ferrag, L. Shu, L. Maglaras, and X. Wang, "Internet of Things for the future of smart agriculture: A comprehensive survey of emerging technologies," *IEEE/CAA J. Automatica Sinica*, vol. 8, no. 4, pp. 718–752, Apr. 2021, doi: 10.1109/JAS.2021.1003925.

[2] F. R. Bassan *et al.*, "Power-over-fiber LPIT for voltage and current measurements in the medium voltage distribution networks," *Sensors*, vol. 21, no. 2, pp. 1–24, 2021, doi: 10.3390/s21020547.

[3] R. A. Khalil, N. Saeed, M. I. Babar, T. Jan, and S. Din, "Bayesian multidimensional scaling for location awareness in hybrid-Internet of Underwater Things," *IEEE/CAA J. Automatica Sinica*, vol. 9, no. 3, pp. 496–509, Mar. 2022, doi: 10.1109/JAS.2021.1004356.

[4] J. D. López-Cardona, D. Sánchez Montero, and C. Vazquez, "Smart remote nodes fed by power over fiber in Internet of Things applications," *IEEE Sensors J.*, vol. 19, no. 17, pp. 7328–7334, Sep. 2019, doi: doi: 10.1109/JSEN.2019.2915613.

[5] S. Heinig, K. Jacobs, S. Norrga, and H.-P. Nee, "Single-fiber combined optical power and data transmission for high-voltage applications," in *Proc. 46th Annu. Conf. IEEE Ind. Electron. Soc. (IECON)*, Oct. 2020, pp. 1473–1480, doi: 10.1109/IECON43393.2020.9255184.

[6] J. Wang *et al.*, "Power-over-fiber technique based sensing system for Internet of Things," in *Proc. 15th Int. Conf. Opt. Commun. Netw. (ICOCN)*, 2016, pp. 1–3, doi: 10.1109/ICOCN.2016.7932370.

[7] J. D. López-Cardona, C. Vázquez, D. S. Montero, and P. C. Lallana, "Remote optical powering using fiber optics in hazardous environments," *J. Lightw. Technol.*, vol. 36, no. 3, pp. 748–754, Feb. 1, 2018, doi: 10.1109/JLT.2017.2776399.

[8] C. Diouf *et al.*, "Design, characterization, and test of a versatile single-mode power-over-fiber and communication system for seafloor observatories," *IEEE J. Ocean. Eng.*, vol. 45, no. 2, pp. 656–664, Apr. 2020, doi: 10.1109/JOE.2018.2876049.

[9] R. Hamié *et al.*, "Experimental characterization of an improved power-over-fiber system for seafloor applications," *Eng. Res. Exp.*, vol. 1, no. 1, 2019, Art. no. 015011, doi: doi: 10.1088/2631-8695/ab30d5.

[10] C. Budelmann, "Opto-electronic sensor network powered over fiber for harsh industrial applications," *IEEE Trans. Ind. Electron.*, vol. 65, no. 2, pp. 1170–1177, Feb. 2018.

[11] J. D. López-Cardona *et al.*, "Optimized power-over-fiber system to remotely feed smart nodes for low-power consumption applications," in *Proc. 13th Spanish Conf. Electron Devices (CDE)*, 2021, pp. 41–44, doi: 10.1109/CDE52135.2021.9455753.

[12] L. C. Souza, E. R. Neto, E. S. Lima, and A. C. S. Junior, "Optically-powered wireless sensor nodes towards industrial Internet of Things," *Sensors*, vol. 22, no. 1, p. 57, 2022, doi: 10.3390/s22010057.

[13] M. A. Bin Rahmat, H. J. Lee, E. Pradana, P. J. Ker, E. M. A. Elsheikh, and P. Thirunavakkarasu, "Development of power over fiber for medical devices application," in *Proc. IEEE 19th Student Conf. Res. Develop. (SCOReD)*, 2021, pp. 367–370, doi: 10.1109/scored53546.2021.9652701.

[14] D. Wake, N. J. Gomes, C. Lethien, C. Sion, and J.-P. Vilcot, "An optically powered radio over fiber remote unit using wavelength division multiplexing," in *Proc. IEEE Int. Meeting Microw. Photon. Jointly Held Asia–Pacific Microw. Photon. Conf. MWP/APMP*, 2008, pp. 197–200, doi: 10.1109/MWP.2008.4666670.

[15] C. Vazquez, D. S. Montero, F. M. A. Al-Zubaidi, and J. D. López-Cardona, "Experiments on shared- and dedicated-power over fiber scenarios in multi-core fibers," in *Proc. Eur. Conf. Netw. Commun. (EuCNC)*, 2019, pp. 412–415, doi: 10.1109/EuCNC.2019.8802042.

Oscar López-Lapeña (Member, IEEE) was born in Barcelona, Spain. He received the M.S. degrees in physics and electronics engineering from the Universitat de Barcelona, Barcelona, Spain, in 1994 and 1996, respectively, and the Ph.D. degree in electronics engineering from the Universitat Politècnica de Catalunya (UPC), Barcelona, in 2000.

Since 2002, he has been an Associate Professor with UPC engaged in teaching on analog and power electronics. His current research interests include low-power converters, control theory, and energy harvesting.

Jose Polo-Cantero received the M.E. degree in telecommunication engineering and the Ph.D. degree from the Universitat Politècnica de Catalunya (UPC), Barcelona, Spain, in 1990 and 2000, respectively.

From 1993 to 1999, he was an Associate Professor with UPC. From 1999 to 2006, he was an Associate Professor with the Universitat Pompeu Fabra, Barcelona. Since 2006, he has been again an Associate Professor with UPC. His current research interests include sensor, sensor networks, mainly wireless networks, and communication standards for wireless sensor network and Internet of Things.